Solar photocatalytic decomposition of estrogens over immobilized zinc oxide

REFERENCE: V. Koutantou, M. Kostadima, E. Chatzisymeon, Z. Frontistis, V. Binas, D. Venieri, D. Mantzavinos, Solar photocatalytic decomposition of estrogens over zinc oxide immobilized on glass substrate, *Catalysis Today* **209** (2012) 66-73. http://dx.doi.org/10.1016/j.cattod.2012.11.004

Solar photocatalytic decomposition of estrogens over immobilized zinc oxide

Virginia Koutantou[1], Maria Kostadima[1], Efthalia Chatzisymeon[1]**, Zacharias Frontistis[1], Vassilios Binas[2], Danae Venieri[1], Dionissios Mantzavinos[1]*

[1] Technical University of Crete, Department of Environmental Engineering, Polytechneioupolis, GR-73100 Chania, Greece

[2] Institute of Electronic Structure and Laser (IESL), FORTH, P.O. Box 1527, Vasilika Vouton, GR-71110 Heraklion, Greece

* First corresponding author:

E-mail: mantzavi@mred.tuc.gr; Tel.: +302821037797; Fax: +302821037857

** Second corresponding author:

E-mail: thalia.chatzisymeon@gmail.com; Tel.: +302821037796; Fax: +302821037857

Abstract

The photocatalytic degradation of synthetic estrogen 17α-ethynylestradiol (EE2) in environmental samples was investigated. Zinc oxide immobilized onto a glass substrate was prepared and used as the photocatalyst, while radiation was provided by a solar simulator. EE2 in the range 50-200 μg/L was treated in various matrices, i.e. ultrapure water, wastewater and drinking water, and treatment efficiency was assessed as a function of photon flux, ZnO loading and addition of hydrogen peroxide. Degradation follows apparent first-order kinetics and increases with increasing photon flux ($4.93\ 10^{-7}$-$5.8\ 10^{-7}$ einstein/(L.s)) and H_2O_2 concentration (up to 100 mg/L), while ZnO loading (1.2-16.3 mg) has a marginal effect. Reaction in ultrapure water is twice as fast as in wastewater (e.g. the respective apparent rate constants are $17.3\ 10^{-3}$ and $9.4\ 10^{-3}$ min^{-1} at maximum photon flux and 3.7 mg ZnO) due to the competition for oxidants between EE2 and the wastewater components (organic matter and ions). The catalyst retained most of its activity upon repeated use (i.e. 21 consecutive runs of 31.5 h duration) although it was partially dissolved in the liquid phase; leached zinc can trigger homogeneous reactions, thus contributing to the overall photocatalytic degradation.

Keywords: EDCs; kinetics; reuse; stability; water matrix; zinc

1. Introduction

Recently, there have been intensive efforts towards the development of efficient technologies for the removal of persistent micro-contaminants from aqueous matrices. Discharges of wastewater treatment plants (WWTPs) typically contain a wide array of such compounds at the ng/L-μg/L levels that have only partially been removed by biological and/or adsorption processes [1]. Endocrine disrupting compounds (EDCs) constitute an important class of such contaminants, which pose an increasing threat to aquatic organisms, as well as to human health. EDCs include naturally occurring estrogens, synthetic estrogens, phyto-estrogens and xeno-estrogens [2]. In particular, the exposure to EDCs has been linked with altering functions of the endocrine system in male fish such as vitellogenin induction and feminized reproductive organs [2]. Moreover, the increasing incidence of cancer and the hypothesis of a decreasing reproductive fitness of men are thought to be attributed

48 to EDCs [3]. Not only this, but it has been found that these compounds can pose a potential danger
49 to fish and other aquatic organisms, even at low concentrations of 0.1-10 ng/L [4]. Thus, it is
50 necessary to develop new and reliable treatment strategies to remove EDCs from wastewaters.
51 Heterogeneous photocatalysis has received enormous attention for the treatment of various classes
52 of organic contaminants found in waters and wastewaters. Titania is by far the most extensively
53 investigated photocatalyst due to its relatively high quantum yield, low cost, elevated stability and
54 availability. Nonetheless, TiO_2 photocatalysis suffers a serious drawback that may restrict its use in
55 large-scale applications, namely its wide band gap energy which overlaps only in the UV region of
56 the electromagnetic spectrum; in this view, the process can utilize only about 6% of the solar energy
57 reaching the earth's surface. An alternative approach is the use of photocatalysts that absorb over a
58 larger fraction of the solar spectrum than TiO_2 and this seems to be the case with ZnO, whose
59 photocatalytic mechanism is similar to that of TiO_2 [5] and also exhibits most of titania's beneficial
60 features possibly with the exception of stability [6]. In several cases, ZnO has shown comparable or
61 even better performance than TiO_2 for the degradation of various contaminants [5, 7-10].
62 Most studies dealing with photocatalytic degradation of pollutants have used semiconductors
63 applied in slurry form into the aqueous phase. However, the major disadvantage of slurry
64 photocatalysis is the inefficient separation of the catalyst from the suspension after treatment. This
65 requires the implementation of a post-treatment recovery step, which would significantly increase
66 treatment cost. Hence, many researchers have focused on immobilizing photocatalysts onto inert
67 surfaces such as glass, cotton or ceramics [11-13].
68 In this work, the photocatalytic degradation of synthetic estrogen 17α-ethynylestradiol (EE2), a
69 major component of the oral contraceptive pill, by simulated solar radiation and in the presence of
70 immobilized ZnO was investigated. The effect of various conditions such as the amount of ZnO
71 attached onto the substrate, photon flux, initial estrogen concentration, treatment time, addition of
72 hydrogen peroxide, presence of other EDCs, and the water matrix was investigated. Moreover, the
73 photocatalytic stability and activity of the prepared catalyst was assessed. To the best of our
74 knowledge, this is the first report on EDCs degradation in environmentally relevant samples by the

proposed photocatalytic system.

2. Materials and methods

2.1 Materials

EE2 and bisphenol-A (BPA) were purchased from Sigma-Aldrich, while ZnO (purity≥99%) from Fluka. $Zn(NO_3)_2.6H_2O$, used as a source of Zn^{2+} for homogeneous photocatalysis, was purchased from Sigma-Aldrich. The water matrix was either of the following: (i) wastewater (WW) collected from the outlet of the secondary treatment of the municipal WWTP of Chania, Greece. The dissolved organic carbon (DOC) was 7.8 mg/L, while the effluent's inherent pH was about 8 and its conductivity was 820 μS/cm; (ii) ultrapure water (UPW) at pH=6.1 taken from a water purification system (EASYpureRF - Barnstead/Thermolyne, USA); (iii) a 50:50 mixture of WW and UPW at pH=7.5; (iv) commercially available bottled water, which will be referred to in the text as drinking water.

2.2 Catalyst preparation

Zinc oxide was immobilized onto glass plates (1.5 cm×1.5 cm) by a heat attachment method. Analytically, the glass plates were previously treated with a 40% HF solution for 90 min and washed with 0.01 M NaOH in order to increase the number of hydroxyl groups and achieve better contact between the catalyst and the glass plates [12]. Moreover, a suspension of 4 g/L ZnO in distilled water was prepared. This suspension was sonicated at 80 kHz for 120 min to improve the dispersion of the solid catalyst in water. Afterwards, the sonicated suspension was poured onto the glass plates at various volumes, ranging from some μL to about 10 mL, and then placed in an oven at 120^{o}C for 60 min. The glass plates were first dried, then fired at 500^{o}C for 180 min and finally washed with distilled water to remove any loosely attached catalytic particles. Scanning electron microscope (SEM) images of the catalytic plates were taken on a JEOL JSM-6400V instrument.

2.3 Photocatalytic experiments

Photocatalytic experiments were performed using a solar simulator (Newport, model 96000) equipped with a 150 W xenon ozone-free lamp and an Air Mass 1.5 Global Filter (Newport, model 81094), simulating solar radiation reaching the surface of the earth at a zenith angle of 48.2°.

The incident radiation intensity on the photochemical reactor in the UV region of the electromagnetic spectrum was measured using 2-nitrobenzaldehyde (purchased from Sigma-Aldrich) as the chemical actinometer [14] and it was found to be 5.8 10^{-7} einstein/(L.s). To assess the effect of intensity on degradation, suitable filters (FSQ-ND04, 50.8 mm×50.8 mm, 0.4 optical density and 39.8% transmittance at 633 nm) were employed to reduce irradiance to 5.4 10^{-7} and 4.93 10^{-7} einstein/(L.s). In a typical photocatalytic run, 64 mL of the water matrix spiked with the appropriate amount of EDC were fed in a cylindrical pyrex cell and the ZnO catalytic plate was added, while the cell was open to the atmosphere. Samples of about 1 mL were periodically taken from the cell and analyzed as follows.

2.4 Analytical methods

HPLC (Alliance 2690, Waters) was employed to monitor the concentrations of EE2 and BPA. Separation was achieved on a Luna C-18(2) column (5 μm, 250 mm×4.6 mm) and a security guard column (4 mm × 3 mm), both purchased from Phenomenex. The mobile phase consisting of 35:65 UPW:acetonitrile eluted isocratically at 1 mL/min and 30°C, while the injection volume was 100 μL. Detection was achieved through a fluorescence detector (Waters 474), in which the excitation wavelength was 280 nm and the emission wavelength was 305 nm. Under these conditions, the retention time for EE2 was 5.1 min, the limit of detection (LOD) was 0.63 μg/L and the limit of quantitation (LOQ) was 2.11 μg/L; the respective values for BPA were 4.3 min, 0.68 μg/L and 2.32 μg/L.

ICP-MS (Agilent Technologies 7500 series) was used to determine the leached zinc concentration in the liquid phase. LOD and LOQ was 1 and 3.32 μg/L, respectively. Residual H_2O_2 concentration was monitored using Merck peroxide test strips in the range 0-100 mg/L.

128

129 **2.5 Yeast estrogen screening (YES) assay**

130 The YES bioassay was carried out as described elsewhere [15, 16]. All chemical ingredients were
131 purchased from Sigma Chemical Company Ltd. (Dorset, England) and were research grade
132 biochemicals suitable for cell culture. Standard 17β-estradiol solutions and sample extracts were
133 produced in ethanol and 10 μL of dilution series were dispensed into triplicate wells of 96-well
134 microtiter plates. The absorbance of the medium was measured using a micro-plate reader (LT-
135 4000MS Microplate Reader, Labtech) and Manta PC analysis software. The absorbance at 540 nm
136 was regarded as estrogenic activity after subtraction of absorbance at 640 nm to correct for yeast
137 growth.

138

139 **3. Results and discussion**

140 **3.1 Effect of ZnO loading**

141 Preliminary experiments were carried out to assess the effect of the amount of immobilized catalyst
142 in the range 1.2-16.3 mg ZnO on 100 μg/L EE2 degradation in UPW. The amount of ZnO that was
143 finally attached onto the glass plate was estimated by weighing the dry glass plate (after treating
144 with HF and washing with NaOH) before and after the deposition and firing of the ZnO powder
145 onto the glass. For ZnO loadings of 1.2, 2.7 and 3.7 mg, the respective EE2 concentration-time
146 profiles matched each other yielding a common conversion of 80% after 90 min (Figure 1).
147 However, increasing ZnO loading to 16.3 mg resulted in a slight conversion decrease to 73%. In a
148 fixed catalyst system, the reactant diffuses from the bulk solution through a boundary layer to reach
149 the liquid-catalyst interface. Subsequently, the reactant molecules diffuse through the catalyst layers
150 to locate active sites where they get adsorbed and react. For immobilized photocatalysts, the
151 optimum film thickness depends on the light penetration depth and the width of the space charge
152 layer. An increase of the catalyst loading increases the degradation rate due to more catalyst surface
153 sites being available for reaction. At the same time, there are two likely loss mechanisms within the
154 catalyst films due to the increase of the catalyst layer thickness that will restrict the presence of

charge carriers at the interface. One is the attenuation of light due to absorption by the catalyst, and the other is the increased probability of charge carrier recombination presumably due to the increased diffusion lengths through the grain boundaries and constrictions within the micro-porous film. Within the bulk of the catalyst film, the extinction of light follows the exponential decay [17]. As the film thickness increases, at some point the penetration depth of light will be such, that most of the electrons and holes are generated relatively close to the solid-liquid interface. The reaction rate will be about maximum at this point. With further increase in the film thickness, the charge carriers are generated relatively far from the liquid-catalyst interface, and consequently, are more susceptible to recombination loss. A further increase of film thickness will then lower the reaction rate.

Figures 2-4 show SEM images of the fresh ZnO catalyst (3.7 mg), as well as at the end of all the photocatalytic runs carried out in this work. Figure 2 shows that the ZnO layer is homogeneous with a porous surface, while the morphology of ZnO particles on the glass surface is amorphous. Moreover, Figure 3 shows SEM images of the cross section of fresh, unused ZnO, while Figure 4 shows SEM images of the cross section of used ZnO. The thickness of fresh catalyst can be estimated between 63 and 74 μm and this decreases in the range 6-24 μm upon repeated use; this is probably due to catalyst leaching as will be discussed in detail in section 3.7.

3.2 Comparison between immobilized and suspended ZnO

To compare the activity between immobilized and suspended ZnO, 1.9, 3.7 or 16.2 mg ZnO were slurried in the reactor. The results are shown in Figure 1, where complete EE2 degradation was achieved after about 60, 40 and 5 min at 1.9, 3.7 and 16.2 mg ZnO, respectively. Conversely, EE2 conversion did not exceed 70-80% after 90 min of reaction with immobilized ZnO. The higher reaction rates achieved in slurry experiments can be attributed to better mixing conditions and the higher diffusion rates of the organics onto the catalyst surface, where they get adsorbed and react. However, the major advantage (i.e. no need for a catalyst recovery step) of the immobilized photocatalysts cannot be overlooked especially if large scale applications are to be considered.

182

183 **3.3 Effect of photon flux**

184 Figure 5 shows concentration-time profiles at photon flux values between 4.93 10^{-7} and 5.8 10^{-7}
185 einstein/(L.s), as well as without irradiation. Degradation decreases with decreasing photon flux,
186 e.g. the 90-min conversion is 80%, 60% and 48% at 5.8 10^{-7}, 5.3 10^{-7} and 4.93 10^{-7} einstein/(L.s),
187 respectively. These findings verify the light-driven nature of the activation of the catalytic process,
188 involving the participation of photogenerated holes and electrons [18]. At relatively low fluxes, the
189 holes, whose concentration is considerably lower than that of photogenerated and n-type electrons,
190 are produced proportionately to the photon flux and depleted to (i) oxidize the contaminants either
191 directly or through the formation of hydroxyl radicals, and (ii) recombine with electrons. In this
192 case, oxidation reactions dominate over recombination and, therefore, their rate is proportional to
193 the photon flux [19]. The initial EE2 degradation rates (i.e. computed over the first 10 min) are
194 1.54, 0.64 and 0.25 μg/(L.min) at 5.8 10^{-7}, 5.3 10^{-7} and 4.93 10^{-7} einstein/(L.s), respectively,
195 showing a linear dependence.

196

197 **3.4 Effect of EE2 concentration**

198 The effect of initial EE2 concentration in the range 50-200 μg/L was investigated and the results are
199 shown in Figure 6. The 90-min conversion becomes 77.3%, 79.4% and 70% at 200, 100 and 50
200 μg/L, respectively, while the corresponding 40-min conversion is 44.1%, 43.2% and 37.5%. The
201 almost stable EE2 conversion irrespective of its initial concentration indicates that degradation
202 follows first-order kinetics, as follows:

203 $$-\frac{d[EE2]}{dt} = k_{app}[EE2] \Leftrightarrow \ln\frac{[EE2]_o}{[EE2]} = k_{app}t \Leftrightarrow \ln(1-X) = -k_{app}t \qquad (1)$$

204 where k_{app} is an apparent reaction rate constant and X is EE2 conversion independent of its initial
205 concentration $[EE2]_o$.

206 The inset of Figure 6 confirms that the reaction approaches, indeed, first-order kinetics. Plotting the
207 logarithm of normalized EE2 concentration against time results in straight lines (the coefficient of

linear regression of data fitting, r^2, is between 98.4% and 99.2%) with a nearly common slope, which corresponds to the apparent reaction rate constant; this is 15.3±2.1 10^{-3} min^{-1}.

3.5 Effect of hydrogen peroxide addition

The addition of H_2O_2 is expected to enhance process efficiency due to its reaction with electrons, i.e.

$$H_2O_2 + e^- \rightarrow {}^{\bullet}OH + OH^- \qquad (2)$$

which reduces the extent of undesired electron-hole recombination and, in parallel, produces extra hydroxyl radicals [20].

As seen in Figure 7, addition of H_2O_2 up to 100 mg/L has a beneficial effect with the e.g. 60-min conversion being 60.4%, 89.2%, 95.8% and 98.9% at 0, 25, 50 and 100 mg/L H_2O_2, respectively. Moreover, there appears to be a linear dependence between the rate and the added peroxide concentration, as clearly seen in the inset of Figure 7; apparent rate constants, computed from the respective EE2 temporal profiles according to eqn (1), take values of 17.3 10^{-3} (r^2=98.8%), 36.5 10^{-3} (r^2=99.9%), 50.7 10^{-3} (r^2=99.5) and 71.8 10^{-3} min^{-1} (r^2=99%) at 0, 25, 50 and 100 mg/L H_2O_2, respectively. It should be noticed here that H_2O_2 was not completely consumed at the end of the 90-min experiment as confirmed using the peroxide test strips; unfortunately, precise determination of residual peroxide was not possible with this method.

3.6 Effect of water matrix

The role of water matrix is crucial since it usually has an adverse effect on treatment efficiency, i.e. it decreases with increasing matrix complexity. This is evident in Figure 8, where the 90-min conversion in WW is only 55%, i.e. 25% less than in UPW. The inset of Figure 8 shows that EE2 degradability decreases in the order UPW (k_{UPW}=17.3 10^{-3} min^{-1}, r^2=98.8%) > Drinking water (k_{DW}=14.7 10^{-3} min^{-1}, r^2=99.4%) > UPW-WW mixture ($k_{UPW\text{-}WW}$=11 10^{-3} min^{-1}, r^2=99.7%) > WW (k_{WW}=9.4 10^{-3} min^{-1}, r^2=99.3%). The fact that reaction rates in WW are nearly twice as slow as in

UPW can be explained taking into account that (i) the oxidizing species are competitively consumed in reactions involving the organic fraction (i.e. about 8 mg/L DOC) inherently present in WW but not in UPW. Since this is known to be refractory to oxidation [21] and constitutes most of the matrix's total content (i.e. 95-99% depending on EE2 initial concentration), photogenerated oxidizing species will partly be wasted attacking this fraction; (ii) hydroxyl radicals may be scavenged by bicarbonates, chlorides and sulfates present in WW (their concentration is in the range 50-250 mg/L). Presumably, the aforementioned arguments are valid for the other two matrices, i.e. drinking water and the UPW-WW mixture where the concentration of matrix species would still be considerable.

Steady-state concentrations of hydroxyl radicals in irradiated suspensions, which contain EE2, can be described as follows [22]:

$$[OH]_{ss} = \frac{I_a \Phi_{OH}}{k_{OH,EE2}[EE2] + \sum k_i [S_i]} \quad (3)$$

where I_a is the rate of light absorption, Φ_{OH} is the apparent quantum efficiency of hydroxyl radical formation, [EE2] and $[S_i]$ are the concentrations of EE2 and all other radical scavengers, respectively, and $k_{OH,EE2}$ and k_i are the second-order rate constants of the reaction of hydroxyl radical with EE2 and S_i, respectively.

If [EE2] is low enough to satisfy the following condition:

$$\sum k_i [S_i] >> k_{OH,EE2}[EE2] \quad (4)$$

the rate of EE2 degradation is a function of the rate of reaction between $OH^{\bullet}$ and EE2, $k_{OH,EE2}$ $[OH]_{ss}$, and the initial concentration of EE2 [22]:

$$\frac{d[EE2]}{dt} = -k_{OH,EE2}[OH]_{SS}[EE2] \quad (5)$$

Using the measured rate constants for EE2 photocatalytic degradation and the known $OH^{\bullet}$ radical rate constant [23], it is possible to mathematically determine the rate of hydroxyl radical formation and, subsequently, $[OH^{\bullet}]_{ss}$ in the aqueous phase.

$$\frac{d[EE2]}{dt} = -k_{app}[EE2] \quad (1)$$

$$[OH]_{ss} = \frac{k_{app}}{k_{OH,EE2}} \quad (6)$$

Under these assumptions, the steady state concentration of hydroxyl radicals is $1.01\ 10^{-10}$, $8.5\ 10^{-11}$, $6.4\ 10^{-11}$ and $5.5\ 10^{-11}$ mol/L for UPW, drinking water, UPW-WW mixture and WW, respectively. Another explanation for the observed matrix effect could be the different pH of UPW and WW affecting the ionization states of EE2 and ZnO surface. EE2 has a pKa value of 10.2 [24], while ZnO has a zero point charge of 9 [25]; therefore, the relative ionization state would not change at the conditions of this work since the matrix pH ranges between 6 and 8 (i.e. ZnO surface is positively charged, while EE2 predominantly occurs at its molecular form).

3.7 ZnO stability and activity

It is well-documented that ZnO stability may be compromised by photo-corrosion, as well as chemical dissolution due to e.g. low pH values [5]. In light of this, several experiments were performed to assess both the photocatalytic activity and stability upon repeated use. Firstly, a freshly prepared plate with a ZnO loading of 3.7 mg was used in three consecutive runs (1st, 2nd and 3rd runs in Figure 9) for the degradation of EE2 in UPW. The plate was then used in several other experiments at various operating conditions, including runs in WW. After extensive use, i.e. 20 runs of 30 h total duration, the plate was tested again for EE2 degradation in UPW (21st run in Figure 9).

As clearly seen in Figure 9, ZnO retains most of its activity upon consecutive use.

Moreover, the concentration of zinc leached into the liquid phase was determined by ICP-MS analysis. About 1.4 mg/L of leached zinc was measured at the end of the first run and about 0.7 mg/L at the end of each of the second and third runs. If all of the metal (i.e. 2.97 mg) were dissolved in the liquid, the resulting concentration would be 46.4 mg/L; therefore, the extent of leaching after the first three runs was 6%. Dissolved zinc was also measured at intermediate runs,

284 e.g. this was 0.15-0.2 mg/L at the end of each of the runs 13th-15th; the fact that the extent of
285 leaching progressively decreases implies that the loosely attached Zn particles have eventually been
286 washed out from the plate. Despite the depletion of zinc from the plate, it is worth noticing that the
287 photocatalytic activity remains outstandingly stable at about 80% upon repeated use. This may be
288 due to (i) the fact that the remaining immobilized catalyst suffices to induce reactions since ZnO
289 loadings in the range 1.2-3.7 mg do not influence activity (see section 3.1); (ii) dissolved zinc
290 initiating homogeneous photocatalytic reactions. To test the latter, an experiment was performed
291 with 1.4 mg/L Zn^{2+} at the conditions of Figure 9; the 90-min conversion was 24% showing that the
292 contribution of homogeneous reactions cannot be disregarded.
293
294 **3.8 Degradation of EDC mixtures**
295 Finally, experiments were carried out to investigate the possible interactions of EE2 with BPA, a
296 xeno-estrogen typically used in the manufacturing of several chemical products that is well-known
297 for its interference with the endocrine system of living beings [3].
298 Figure 10a shows EE2 concentration-time profiles (50-200 μg/L initial concentration) in UPW and
299 in the presence of 100 μg/L BPA, while Figure 10b shows BPA concentration-time profiles (100
300 μg/L initial concentration) in UPW and in the presence of different EE2 concentrations in the range
301 0-200 μg/L. Comparing Figures 6 and 10a, it is deduced that EE2 degradation is not impeded by the
302 presence of BPA (on the contrary, it is slightly enhanced in certain cases); on the other hand, Figure
303 10b shows an inhibition of BPA degradation from 76% after 90 min in the absence of EE2 to
304 48±5% in the presence of 50-200 μg/L EE2. A possible explanation would involve differences in
305 their chemical structures (shown in Figure 10b). EE2 has a longer molecular chain with more
306 complicated structure than BPA and this could render it more readily susceptible to oxidative
307 attack. In addition, the simultaneous BPA degradation may create active radicals that would also
308 attack EE2, facilitating thus its degradation. On the other hand, EE2 may act as a shield to BPA
309 molecule preventing its diffusion to the catalyst surface, thus decreasing its degradability.

310 The experiments were then performed in WW and the results are shown in Figure 11. EE2
311 degradation is again enhanced in the presence of BPA, as seen from Figures 8 and 11a. Conversely,
312 the effect of EE2 on BPA is less pronounced (Figure 11b) than in UPW but this is because the WW
313 matrix has already had a strong adverse impact for the reasons discussed in section 3.6 (e.g. the 90-
314 min BPA conversion without EE2 decreased from 76% in UPW to 45% in WW).
315 A kinetic simulation of EE2 degradation in the presence of BPA was performed both for UPW and
316 WW matrices. Based on the experimental data shown in Figures 10a and 11a, it seems that EE2
317 reduction deviates from first-order kinetics as its degradation rate depends on its initial
318 concentration. Therefore, a zero-order kinetic expression was applied to simulate the process:

319 $$-\frac{d[EE2]}{dt} = k'_{app} \Leftrightarrow [EE2]_0 - [EE2] = k'_{app} t \qquad (7)$$

320 where k'_{app} is an apparent reaction constant. If the data of Figure 10a are plotted in the form of eqn.
321 (7), straight lines (shown in the inset graph) passing through the origin fit the experimental results
322 well (the coefficient of linear fitting, r^2, is 0.935, 0.993 and 0.996) and from the slopes of the
323 straight lines the computed constants are 0.004, 0.013 and 0.023 μg/(L.min) when the initial
324 concentration of EE2 is 50, 100 and 200 μg/L, respectively.
325 If the data of Figure 11a are treated in a similar way, respective kinetic constants can be computed
326 for EE2 degradation as follows: 0.004 (0.989), 0.012 (0.992) and 0.016 μg/(L.min) (0.994) for 50,
327 100 and 300 μg/L EE2, respectively, with numbers in brackets corresponding to fitting coefficients.
328 Interestingly, when EE2 is found in a mixture with other organic substances, such as BPA, then its
329 degradation rate follows different order kinetics implying that the complex matrix of environmental
330 wastewater samples should be taken into consideration.
331 Finally, the estrogenic activity of the samples before and after photocatalytic treatment was
332 measured showing that photocatalysis over immobilized ZnO is capable of reducing estrogenicity of
333 environmental water and wastewater samples. Specifically, it was found that the estrogenic activity
334 of the UPW mixture containing 100 μg/L of BPA and EE2 decreased by 50.3%, while the
335 respective value for the WW matrix was only 13.5%, reflecting once again the importance of the

336 complexity of the water matrix.

337

338 **4. Conclusions**

339 The degradation of estrogen EE2 driven by simulated solar radiation over immobilized ZnO
340 photocatalyst was investigated. Although reactions in slurry systems are considerably faster than
341 with immobilized catalysts, the former would require extra processes for catalyst recovery and
342 reuse. In addition, the use of renewable energy source is conceptually advantageous. The main
343 conclusions extracted from this work are as follows:

344 1) Degradation in the range 50-200 μg/L EE2 can be modelled by first order kinetics. At the
345 conditions employed in this study, rates increase linearly with increasing photon flux and the
346 concentration of added H_2O_2.

347 2) The more complex the water matrix is the slower EE2 degradation becomes; this is due to the
348 non-target species inherently present in the matrix behaving as scavengers of the photogenerated
349 oxidants. Nevertheless, the presence of BPA spiked in the reaction mixture did not obstruct
350 degradation, although it altered kinetics.

351 3) Catalyst activity and stability are key issues in developing efficient catalytic processes. At the
352 conditions in question, ZnO retained its activity on repeated use (e.g. after 21 consecutive runs,
353 50% of which were performed in WW containing lots of impurities, natural organic matter and
354 salts). This said, partial metal leaching was recorded that may contribute to degradation through
355 homogeneous photocatalytic reactions.

356

357 **Acknowledgements**

358 The authors thank (i) Ms L. Saru (Technical University of Crete) for performing ICP-MS analysis,
359 and (ii) Dr. E. Routledge (Institute for the Environment, Brunel University, UK) for kindly
360 providing the recombinant yeast.

361

362 **References**

363 1. M. Klavarioti, D. Mantzavinos, D. Kassinos, Environ. Intern. 35 (2009) 402-417.

364 2. M. Auriol, Y. Filali-Meknassi, R.D. Tyagi, C.D. Adams, R.Y. Surampalli, Process Biochem. 41
365 (2006) 525-553.

366 3. P.K. Jjemba, Pharma-ecology. The Occurrence and Fate of Pharmaceuticals and Personal Care
367 Products in the Environment American Water, Deltran, John Wiley & Sons, New Jersey, 2008.

368 4. V. Belgiorno, L. Rizzo, D. Fatta, C. Della Rocca, G. Lofrano, A. Nikolaou, V. Naddeo, S.
369 Meric, Desalination 215 (2007) 166-176.

370 5. Z. Frontistis, D. Fatta-Kassinos, D. Mantzavinos, N.P. Xekoukoulotakis, J. Chem. Technol.
371 Biotechnol. 87 (2012) 1051-1058.

372 6. N. Morales-Flores, U. Pal, E.M. Sanchez, Appl. Catal. A-Gen. 394 (2011) 269-275.

373 7. R. Al-Rasheed, D.J. Cardin, Appl. Catal. A-Gen. 246 (2003) 39-48.

374 8. S.K. Kansal, M. Singh, D. Sud, J. Hazard. Mater. 141 (2007) 581-590.

375 9. I. Poulios, M. Kositzi, A. Kouras, J. Photoch. Photobiol. A 115 (1998) 175-183.

376 10. P.R. Shukla, S. Wang, H.M. Ang, M.O. Tade, Sep. Purif. Technol. 70 (2010) 338-344.

377 11. A.R. Khataee, Environ. Technol. 30 (2009) 1155-1168.

378 12. M.A. Behnajady, N. Modirshahla, N. Daneshvar, M. Rabbani, J. Hazard. Mater. 140 (2007)
379 257-263.

380 13. V.M. Daskalaki, Z. Frontistis, D. Mantzavinos, A. Katsaounis, Catal. Today 161 (2011) 110-
381 114.

382 14. E.S. Galbavy, K. Ram, C. Anastasio, J. Photoch. Photobiol. A 209 (2010) 186-192.

383 15. E.J. Routledge, J.P. Sumpter, Environ. Toxicol. Chem. 15 (1996) 241-248.

384 16. P. De Boever, W. Demaré, E. Vanderperren, K. Cooreman, P. Bossier, W. Verstraete, Environ.
385 Health Perspect. 109 (2001) 691-697.

386 17. K. Mehrotra, G.S. Yablonsky, A.K. Ray, Chemosphere 60 (2005) 1427-1436.

387 18. J-M. Herrmann, Appl. Catal. B-Environ. 99 (2010) 461-468.

388 19. S. Malato, P. Fernandez-Ibanez, M.I. Maldonado, J. Blanco, W. Gernjak, Catal. Today 147

(2009) 1-59.

20. F. Mendez-Arriaga, S. Esplugas, J. Gimenez, Water Res. 44 (2010) 589-595.
21. Z. Frontistis, N.P. Xekoukoulotakis, E. Hapeshi, D. Venieri, D. Fatta-Kassinos, D. Mantzavinos Chem. Eng. J. 176 (2011) 175-182.
22. H. Kawaguchi, Chemosphere 22 (1991) 1003-1009.
23. B.A. Wols, C.H.M. Hofman-Caris, Water Res. 46 (2012) 2815-2827.
24. H. Fu, R.P. Suri, R.F Chimchirian, E. Helmig, R. Constable, Environ. Sci. Technol. 41 (2007) 5869-5874.
25. S. Sakthivel, B. Neppolian, M.V. Shankar, B. Arabindoo, M. Palanichamy, V. Murugesan, Sol. Energ. Mat. Sol. C. 77 (2003) 65-82.

401 **List of Figures**

402

403 **Figure 1.** Effect of ZnO loading on EE2 degradation in immobilized and suspended systems.
404 Conditions: $[EE2]_0$=100 μg/L; Photon flux=5.8 10^{-7} einstein/(L.s); Matrix: UPW.

405 **Figure 2.** SEM images of (a) fresh and (b) used ZnO catalyst for EE2 degradation.

406 **Figure 3.** Cross section SEM images of fresh ZnO catalyst. The thickness is (a) 74.3 μm and (b) 63
407 μm.

408 **Figure 4.** Cross section SEM images of used ZnO catalyst. The thickness is between (a) 14-24 μm
409 and (b) 6-7 μm.

410 **Figure 5.** Effect of photon flux on EE2 degradation. Conditions: ZnO=3.7 mg; $[EE2]_0$=100 μg/L;
411 Matrix: UPW.

412 **Figure 6.** Effect of initial EE2 concentration on its degradation. Inset graph: Plot of eqn (1).
413 Conditions: ZnO=3.7 mg; Photon flux=5.8 10^{-7} einstein/(L.s); Matrix: UPW.

414 **Figure 7.** Effect of hydrogen peroxide on EE2 degradation. Inset graph: Relationship between rate
415 constant and H_2O_2. Conditions: ZnO=3.7 mg; $[EE2]_0$=100 μg/L; Photon flux=5.8 10^{-7} einstein/(L.s);
416 Matrix: UPW.

417 **Figure 8.** Effect of water matrix on EE2 degradation. Inset graph: Relationship between rate
418 constant and matrix. Conditions: ZnO=3.7 mg; $[EE2]_0$=100 μg/L; Photon flux=5.8 10^{-7}
419 einstein/(L.s).

420 **Figure 9.** ZnO activity upon repeated use. Conditions: ZnO=3.7 mg; $[EE2]_0$=100 μg/L; Photon
421 flux=5.8 10^{-7} einstein/(L.s); Matrix: UPW.

422 **Figure 10.** Behavior of EE2 and BPA mixtures in UPW. Effect of (a) 100 μg/L BPA on 50-200
423 μg/L EE2 degradation. Inset graph: Plot of eqn (7); (b) 50-200 μg/L EE2 on 100 μg/L BPA
424 degradation. Conditions: ZnO=3.7 mg; Photon flux=5.8 10^{-7} einstein/(L.s).

425 **Figure 11.** Behavior of EE2 and BPA mixtures in WW. Effect of (a) 100 μg/L BPA on 50-300 μg/L
426 EE2 degradation. Inset graph: Plot of eqn (7); (b) 50-300 μg/L EE2 on 100 μg/L BPA degradation.
427 Conditions: ZnO=3.7 mg; Photon flux=5.8 10^{-7} einstein/(L.s).

428

429

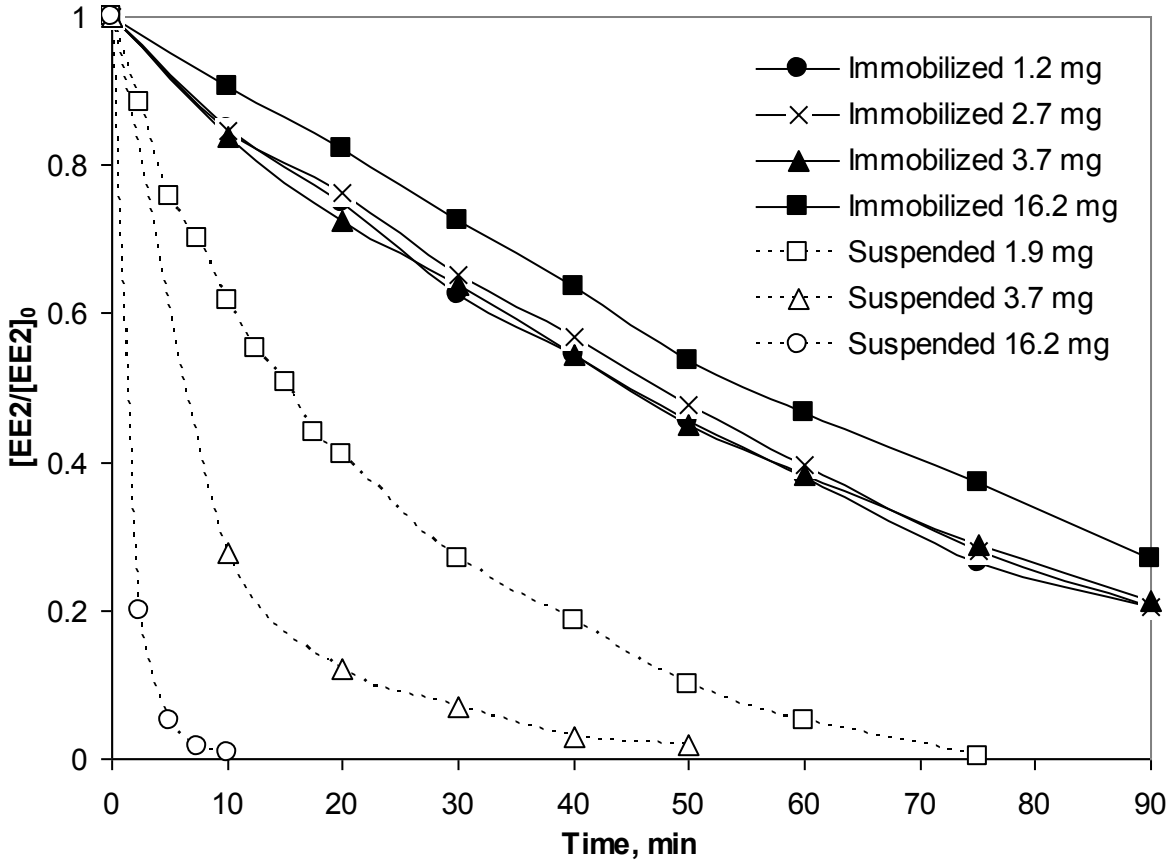
Immobilized 1.2 mg
Immobilized 2.7 mg
Immobilized 3.7 mg
Immobilized 16.2 mg
Suspended 1.9 mg
Suspended 3.7 mg
Suspended 16.2 mg
[EE2/[EE2]0
Time, min
0
0.2
0.4
0.6
0.8
1
0
10
20
30
40
50
60
70
80
90

Figure 1.

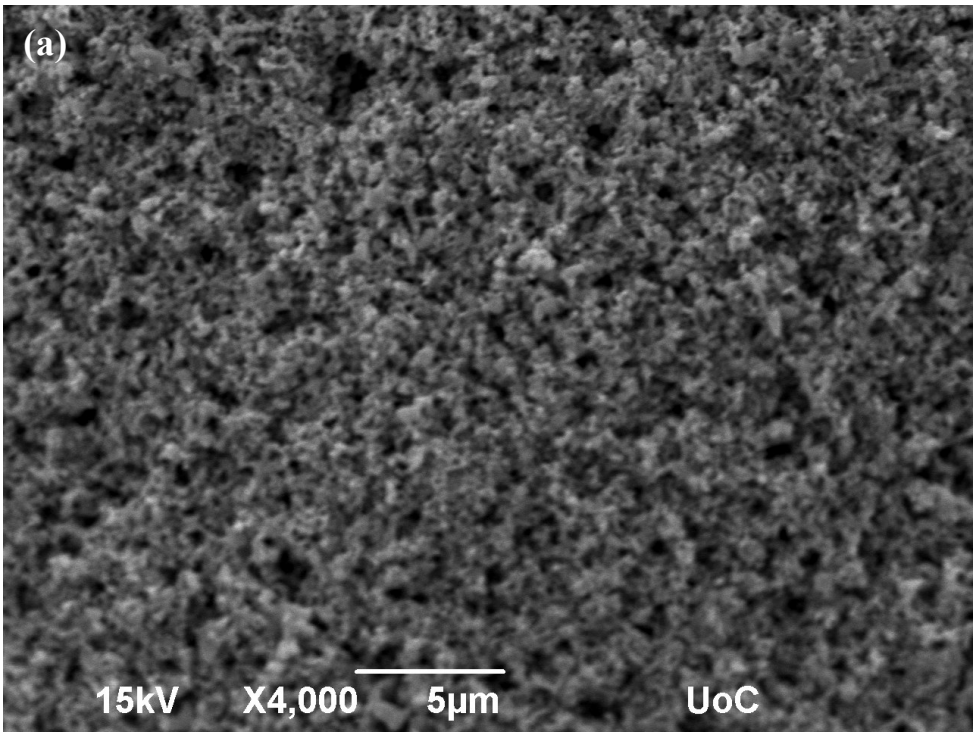

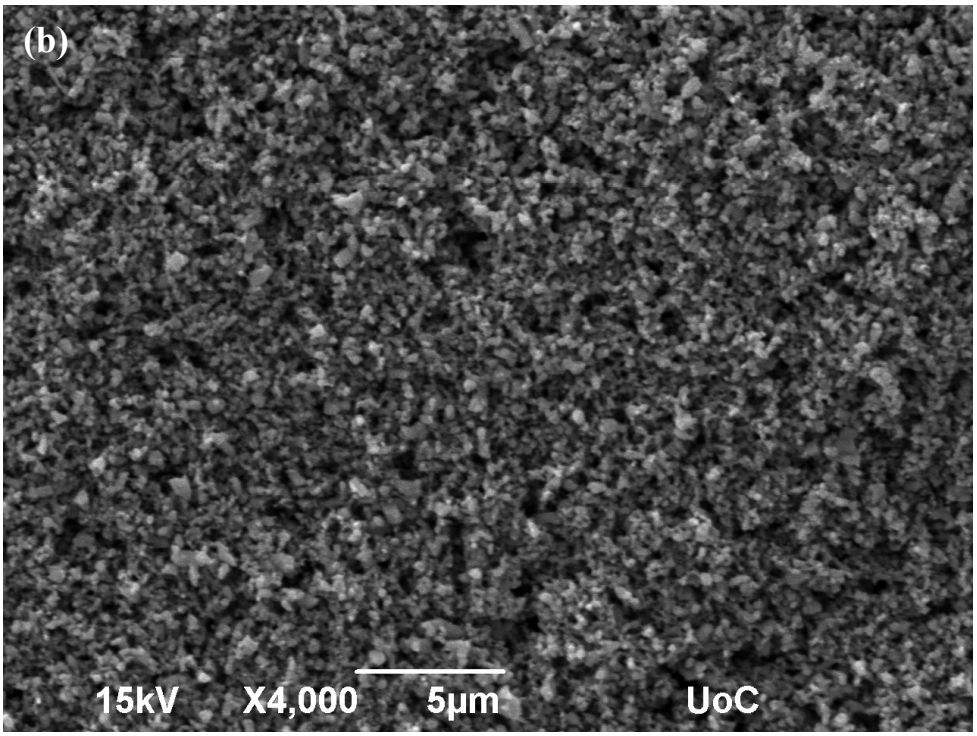

Figure 2.

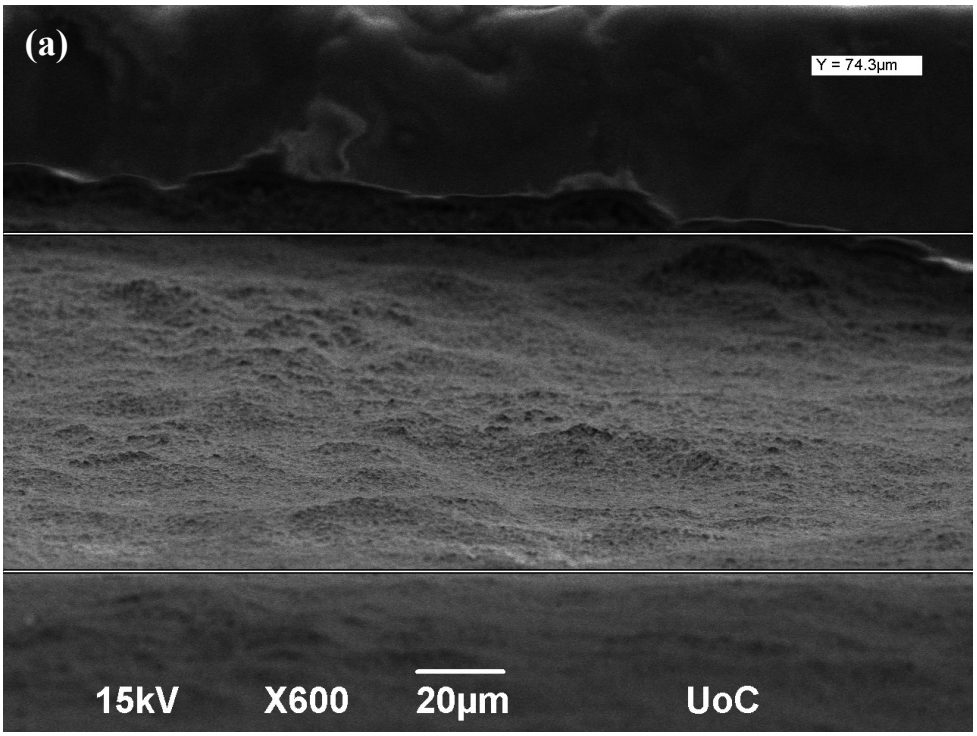

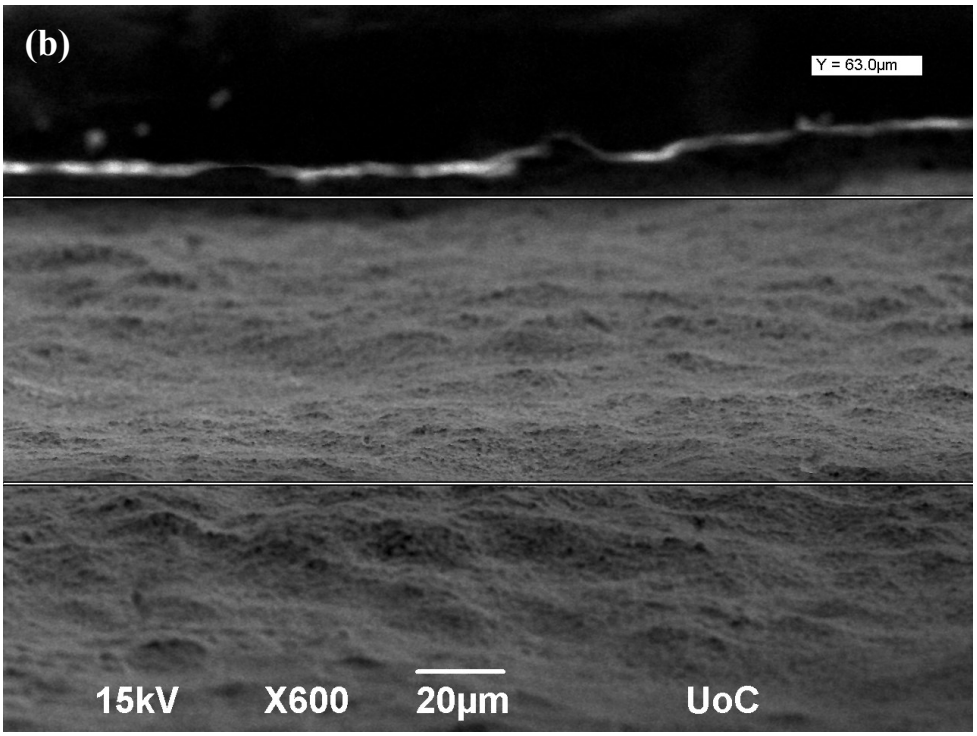

Figure 3.

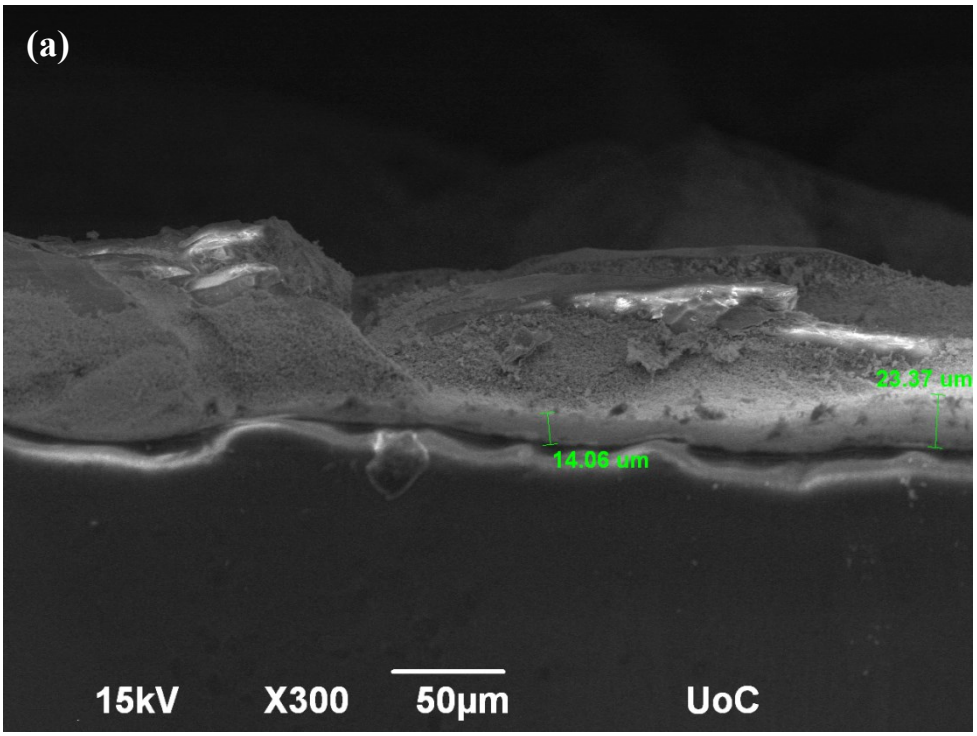
(a)
23.37 um
14.06 um
15kV X300 50µm UoC

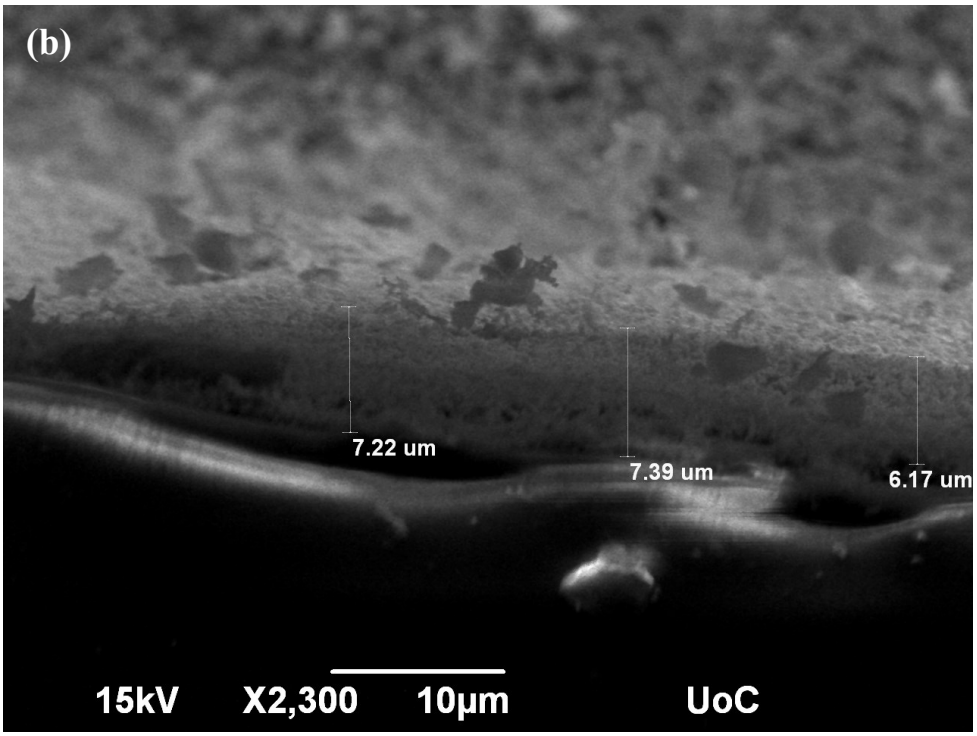
(b)
7.22 um
7.39 um
6.17 um
15kV X2,300 10µm UoC

Figure 4.

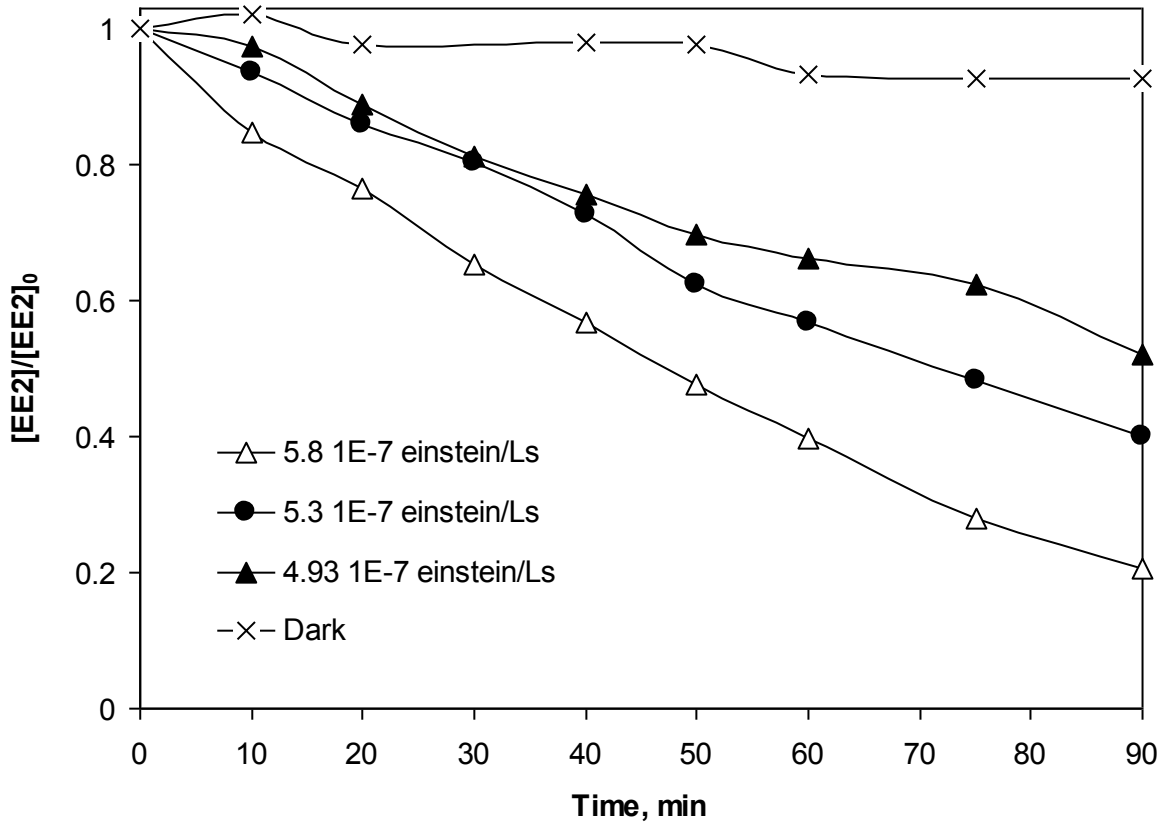
[EE2]/[EE2]0
1
0.8
0.6
0.4
0.2
0
0
10
20
30
40
50
60
70
80
90
Time, min
5.8 1E-7 einstein/Ls
5.3 1E-7 einstein/Ls
4.93 1E-7 einstein/Ls
Dark

Figure 5.

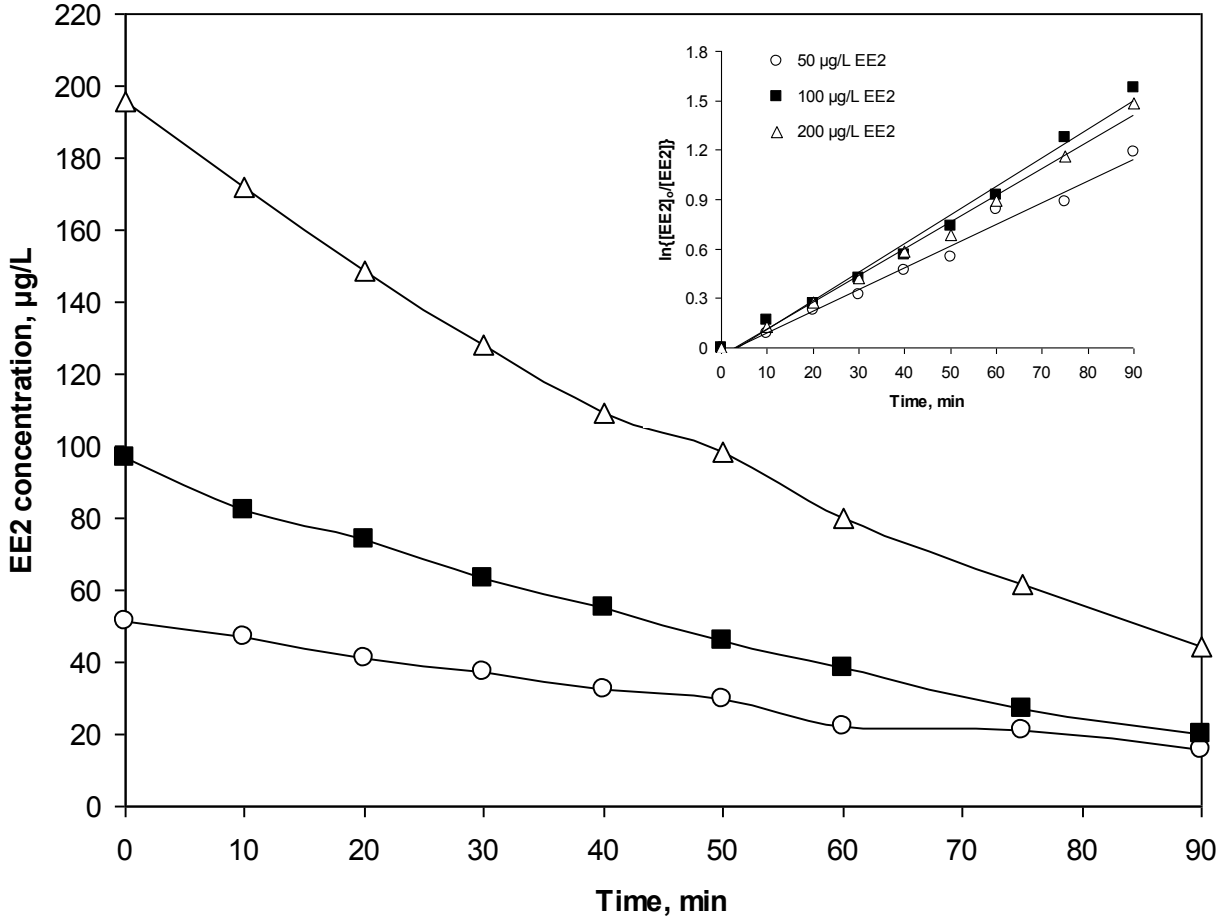
EE2 concentration, µg/L
Time, min
50 µg/L EE2
100 µg/L EE2
200 µg/L EE2
ln{[EE2]o/[EE2]}
Time, min

Figure 6.

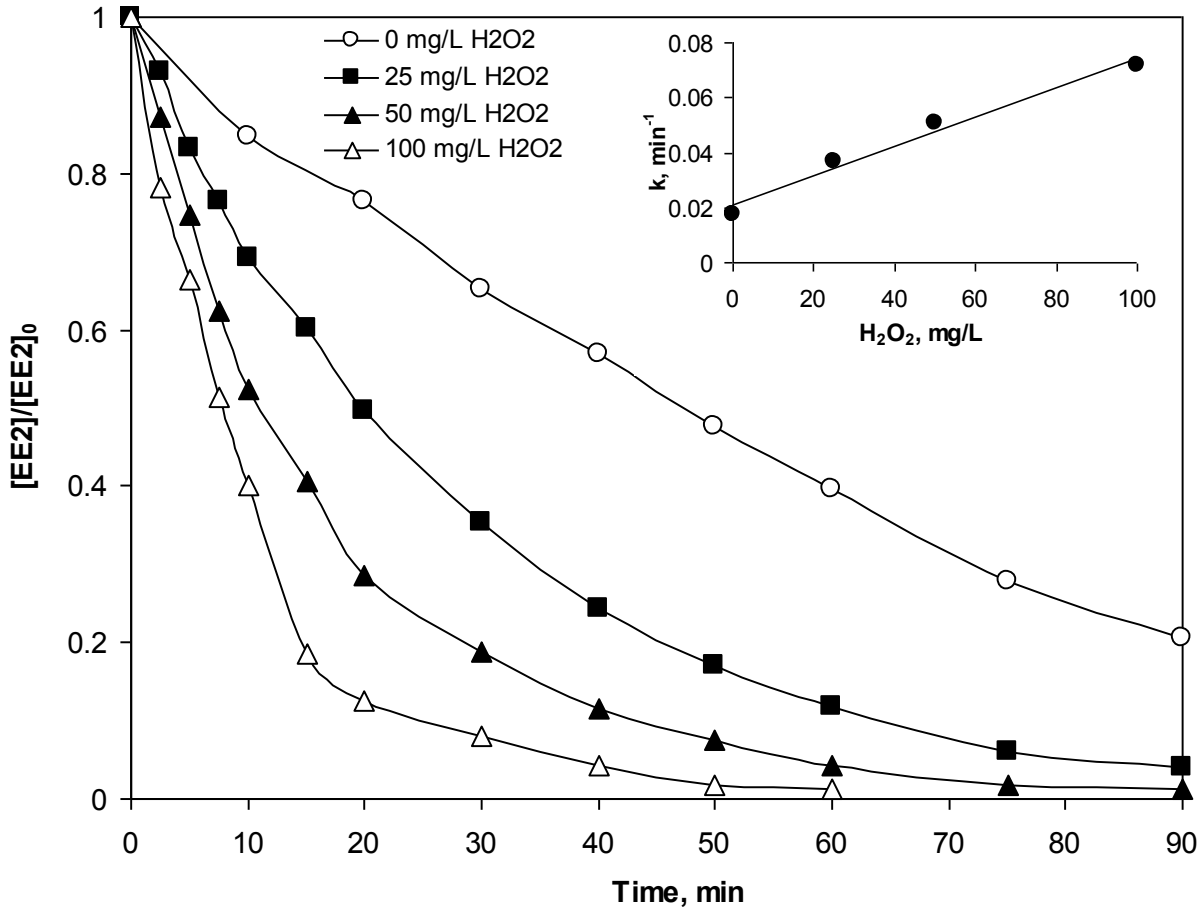
0 mg/L H2O2
25 mg/L H2O2
50 mg/L H2O2
100 mg/L H2O2
[EE2]/[EE2]0
Time, min
k, min-1
H2O2, mg/L

Figure 7.

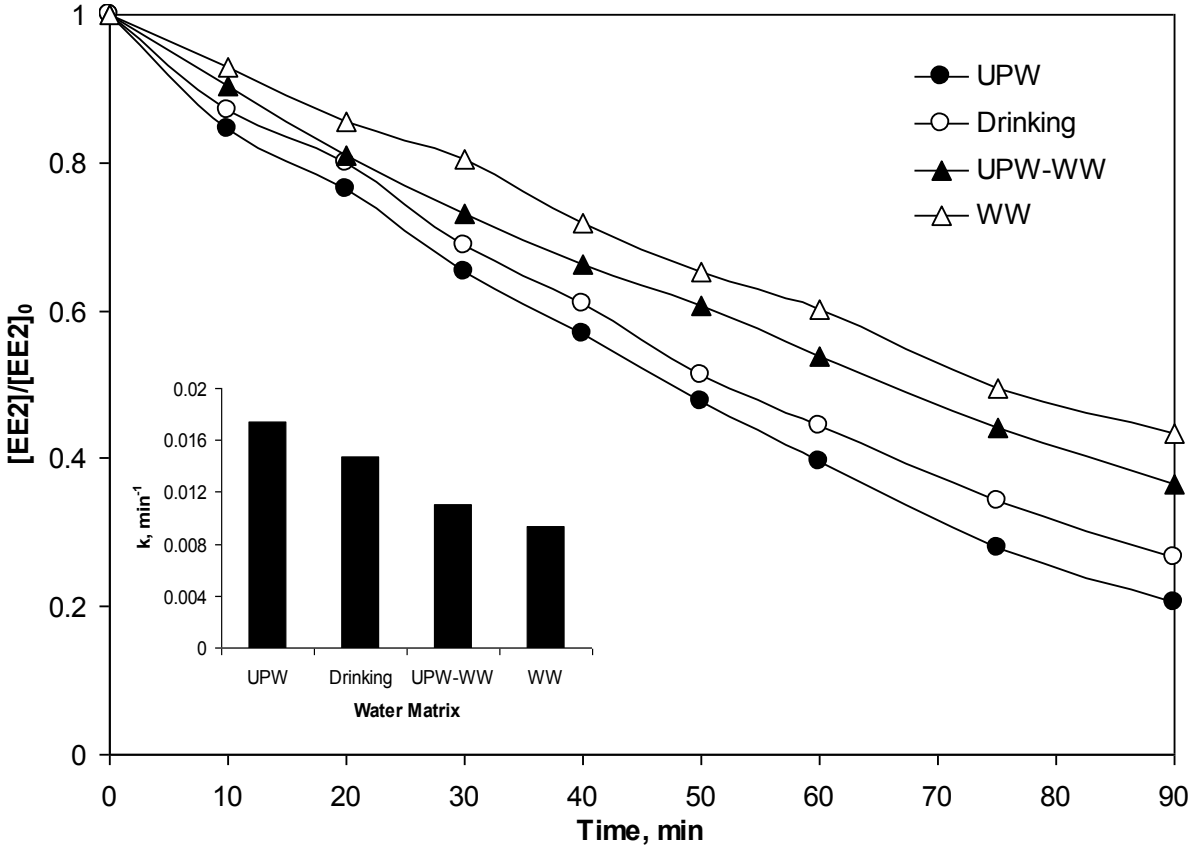
UPW
Drinking
UPW-WW
WW
[EE2]/[EE2]0
Time, min
k, min-1
Water Matrix
UPW
Drinking
UPW-WW
WW

Figure 8.

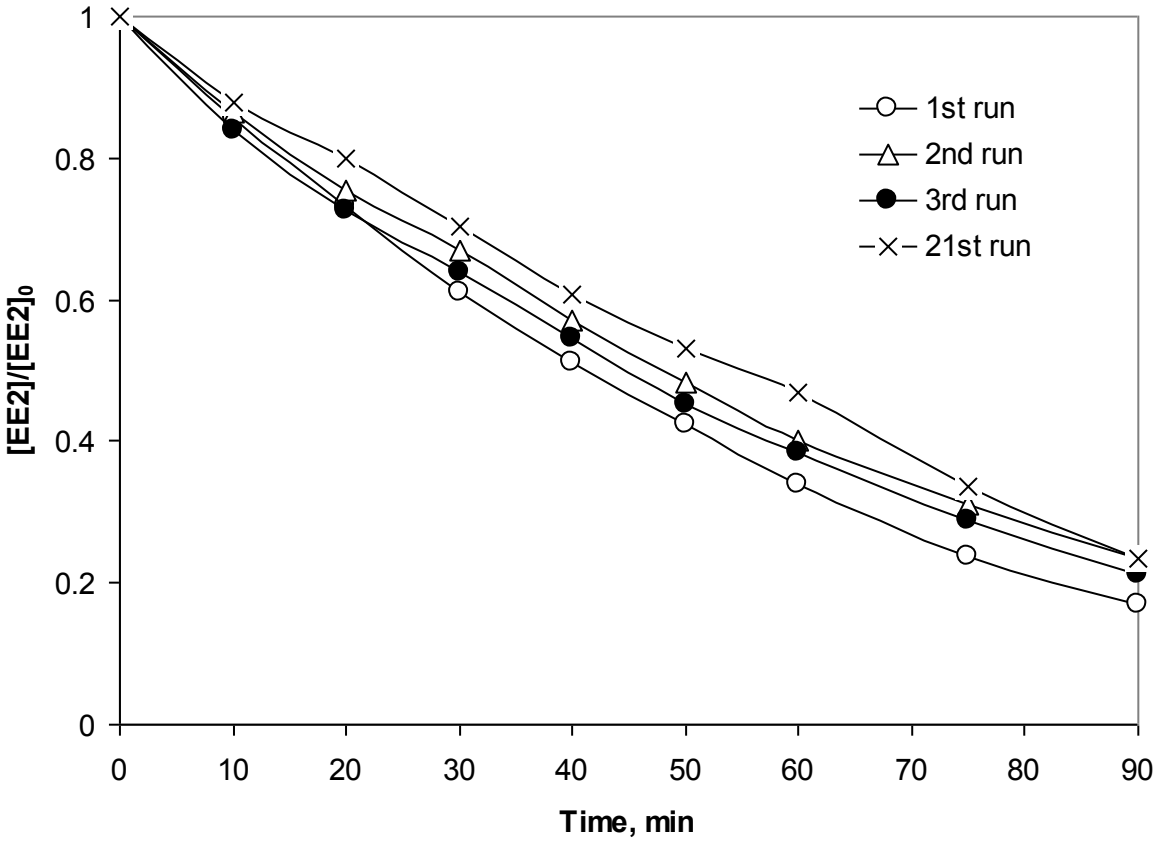
1st run
2nd run
3rd run
21st run
[EE2]/[EE2]0
Time, min
0
0.2
0.4
0.6
0.8
1
0
10
20
30
40
50
60
70
80
90

Figure 9.

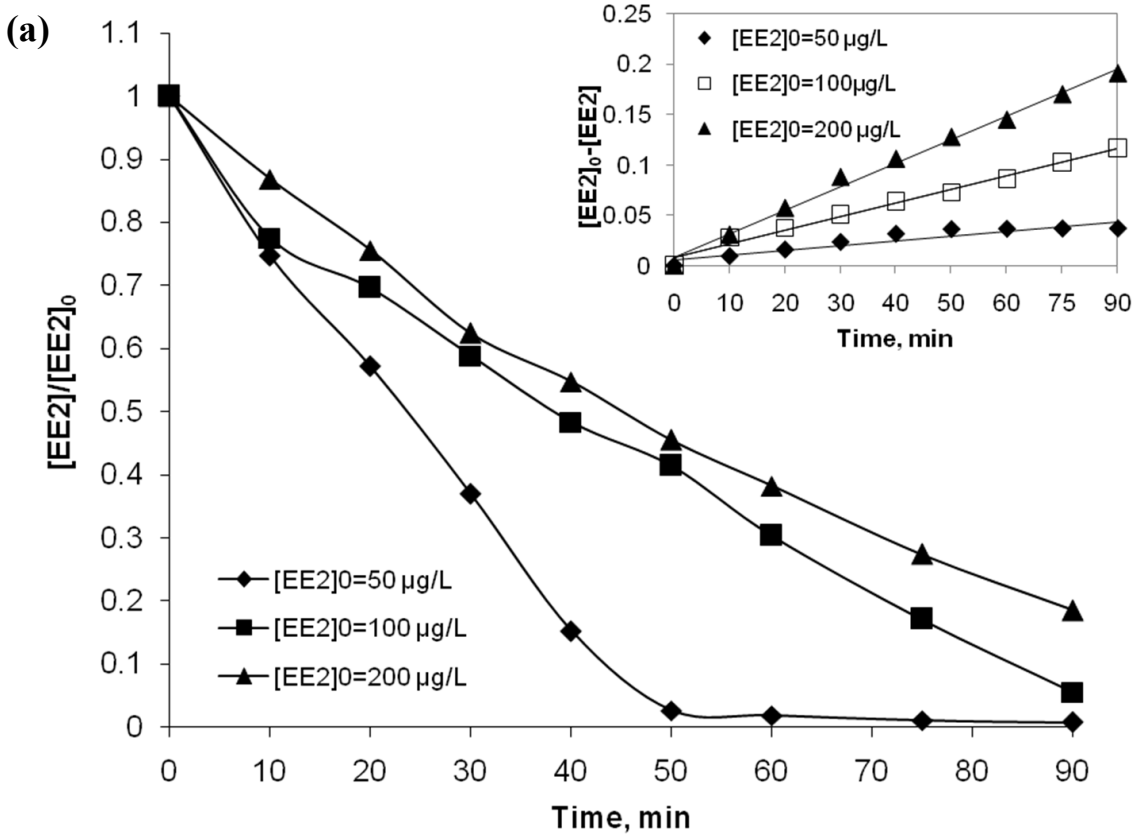

553

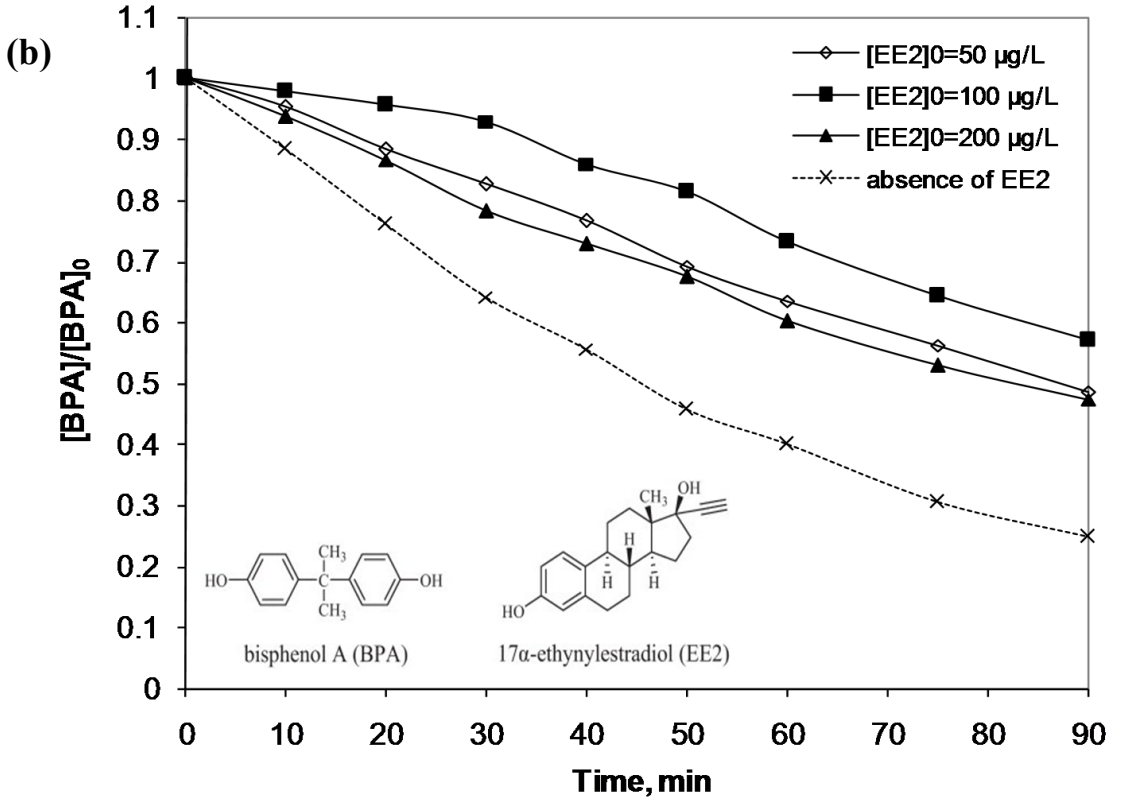

554

555 Figure 10.

556

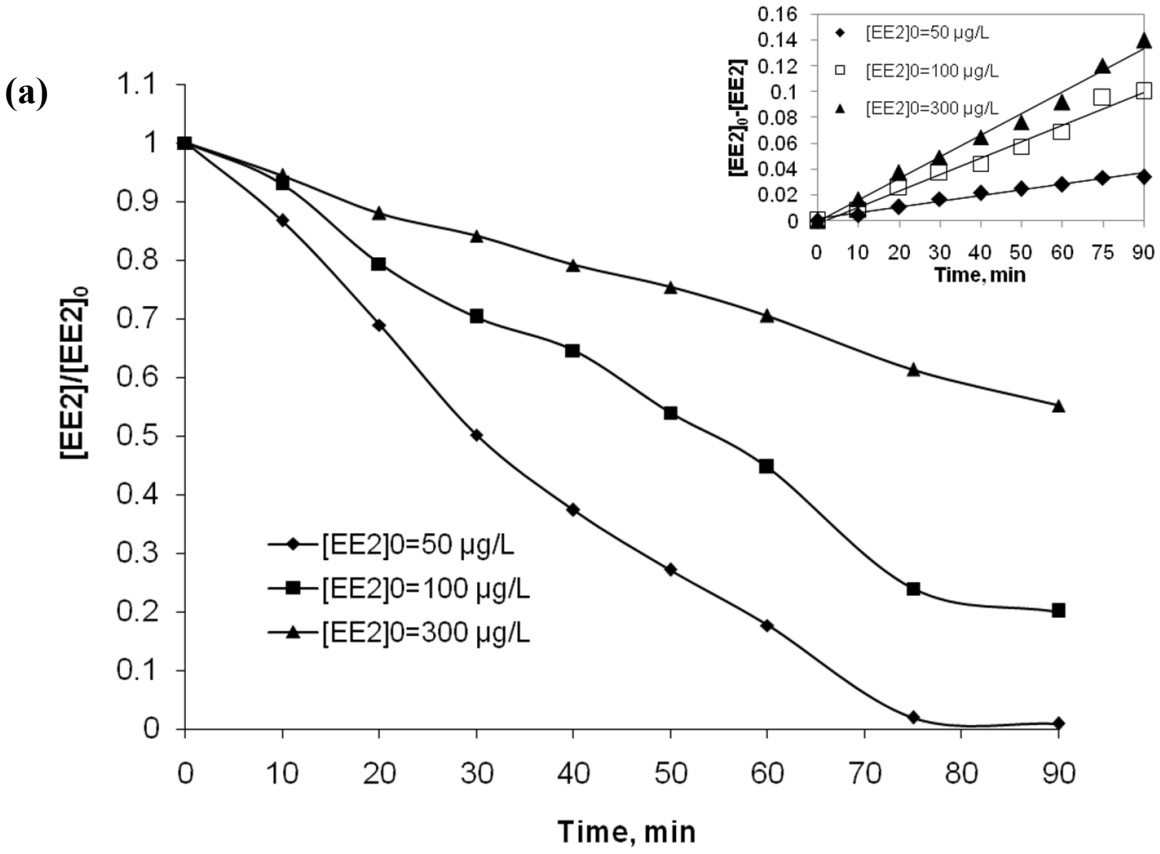
(a)
[EE2]/[EE2]0
Time, min
[EE2]0=50 µg/L
[EE2]0=100 µg/L
[EE2]0=300 µg/L
[EE2]0-[EE2]
Time, min
[EE2]0=50 µg/L
[EE2]0=100 µg/L
[EE2]0=300 µg/L

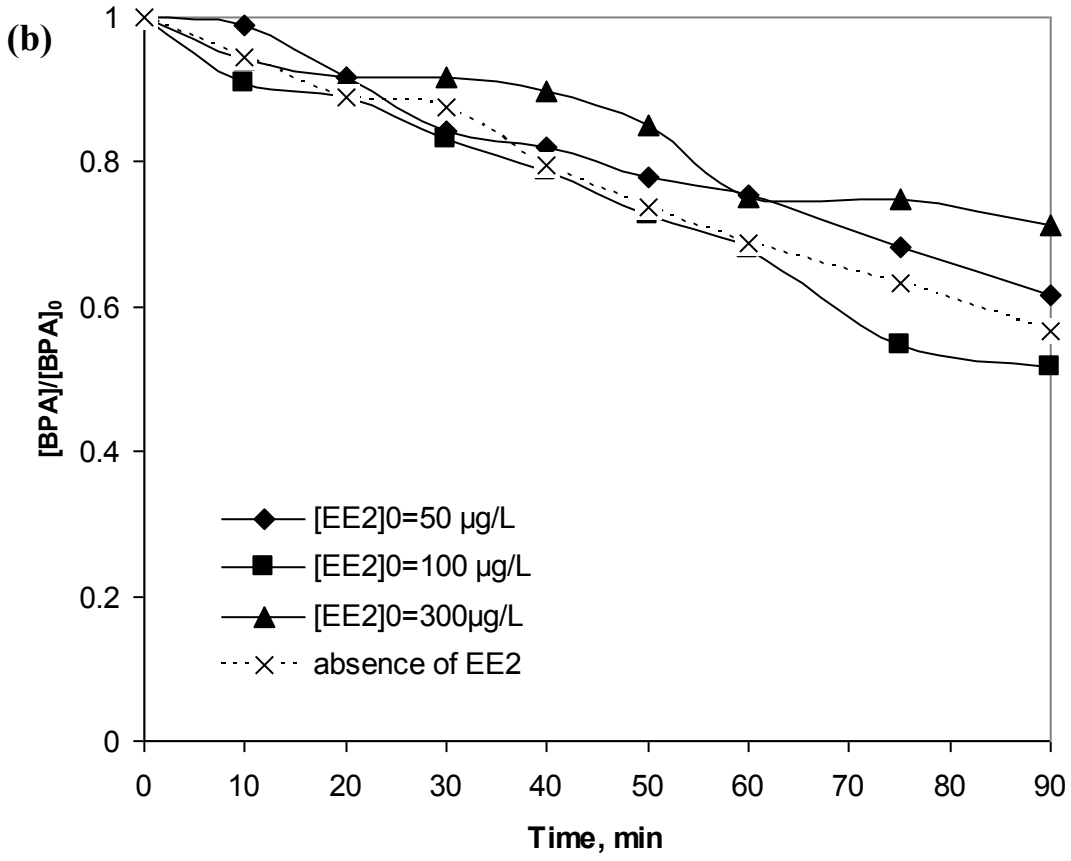
(b)
[BPA]/[BPA]0
Time, min
[EE2]0=50 µg/L
[EE2]0=100 µg/L
[EE2]0=300µg/L
absence of EE2

Figure 11.